Classical impulse approximation for the electron loss from H(1s) or H^- projectiles passing through various gas targets

K. Riesselmann, L. W. Anderson, and L. Durand
Department of Physics, University of Wisconsin–Madison, Madison, Wisconsin 53706

C. J. Anderson
IBM Thomas J. Watson Research Center, Yorktown Heights, New York 10598
(Received 20 August 1990; revised manuscript received 12 February 1991)

This paper presents calculations of electron-loss cross sections for fast H(1s) projectiles incident on different atomic targets (He, Ne, Ar, Kr, Xe, H, N, or O) for a broad kinetic-energy range (90 keV/amu to 1.4 GeV/amu), and compares the calculations with experimental measurements where possible. The calculations are based on the semiclassical free-collision model. Theoretical differential cross sections for elastic electron scattering, and theoretical or semiempirical differential cross sections for inelastic electron scattering, are used in making the calculations. The results are in good agreement with experimental data. We apply a simple model based on the H(1s) results to obtain single- and double-electron-loss cross sections for H^- projectiles incident on the same atomic targets. Again the results are in good agreement with experiment. Further calculations have yielded results for electron loss of H(1s) incident on molecular H_2, N_2, and O_2 targets.

I. INTRODUCTION

Electron-detachment cross sections are of interest both intrinsically and for a variety of applications. For example, at incident energies above about 100 keV/amu, the best method for producing fast neutral hydrogen (or deuterium or tritium) atoms is to accelerate H^- ions to high energy and detach one of the electrons.[1] Fast neutral atomic beams are used for heating controlled thermonuclear plasmas. Another application of electron detachment is the production of polarized positive hydrogen ions, which can be formed by the pick up of a polarized electron, the transfer of the electron polarization to the nucleus, and the subsequent collisional detachment of the electron.[2–8]

This paper reports calculations of the electron-loss cross sections for fast H(1s) atoms incident on He, Ne, Ar, Kr, Xe, H, N, or O atomic targets as a function of the energy of the incident fast H(1s) atom for energies in the range 90 keV/amu to 1.4 GeV/amu. Also reported are calculations of single- and double-electron-loss cross sections for fast H^- ions incident on the same gas targets as a function of the incident energy for the same energy range. Completely quantum-mechanical calculations of these cross sections are difficult. Instead, we further develop a simple semiclassical model to calculate these cross sections from known electron-scattering cross sections. The results of our calculations are compared to experimental measurements of these cross sections where possible. The calculations show good agreement with the measured cross sections.

To describe the loss of the single electron from H(1s), we utilize an extension of the semiclassical free-collision model.[9–11] The electron in the H(1s) atom is treated as a free electron with a velocity that is equal to the velocity of the H(1s) center-of-mass velocity plus the velocity of the electron about the H(1s) center of mass. The electron is assumed to be scattered by a target atom with a cross section equal to that for a free electron. The scattering of the hydrogen nucleus is neglected. In order for the electron to be detached, it must receive an impulse during the collision that is large enough that it acquires an energy greater than the ionization energy for the H(1s) atom. This condition restricts the allowed kinematic configurations, and requires that the free-electron scattering angle be larger than a critical angle θ_c which depends on the other kinematic variables. Our calculations show that it is important to include this effect, and to average over the initial electron velocities in the incident atom.

A geometrical model[10,12] in combination with the free-collision model is also used to calculate electron-loss cross sections for incident H^- ions. Using a true three-dimensional model, we calculate not only single- but also double-electron-loss cross sections. The geometrical model presented is valuable because it affords a relatively simple semiclassical method to utilize known electron-scattering cross sections to calculate the one- or two-electron-detachment cross sections.

Finally, we use the geometrical model and our semiclassical electron-loss cross section for H(1s) incident on single atoms to calculate the electron-loss cross sections for H(1s) incident on diatomic homonuclear targets. The molecular cross sections approach twice the atomic cross sections at high energies, but the molecular-to-atomic ratio falls significantly below 2 at low energies. The results are in excellent agreement with existing data.

II. METHOD OF THE CALCULATIONS FOR A H(1s) PROJECTILE

The calculations are carried out using a free-collision classical-impulse approximation. In this formalism the

projectile and electron velocities are used as the variables. These velocities are more suitable variables than the projectile and electron kinetic energies, which include the different masses. The velocities describing the scattering process in this approximation are shown in Fig. 1. The velocity of the center of mass of the incident hydrogen atom is denoted as $\mathbf{v}_N$. The velocity of the electron with respect to the center of mass of the incident hydrogen atom is $\mathbf{u}_i$. The angle β between $\mathbf{v}_N$ and $\mathbf{u}_i$ is arbitrary. Eventually we average over all values of β. With respect to the laboratory frame, in which the target is at rest, the electron is incident on the target atom with a velocity $\mathbf{v}_i$, which in the nonrelativistic case is given by $\mathbf{v}_i=\mathbf{v}_N+\mathbf{u}_i$. The electron is scattered impulsively by the target. In particular, we neglect interactions between the electron and the hydrogen nucleus during the electron-atom collision. The electron velocity just after the collision has occurred is denoted by $\mathbf{v}_f$. Assuming that the scattering of the nucleus of the projectile is small, we take the final velocity of the hydrogen nucleus to be equal to the initial velocity of the hydrogen nucleus, so that both are approximately equal to $\mathbf{v}_N$. The assumption of negligible scattering of the nucleus also implies that any change in the internal energy of the target, ΔE, is solely related to a change in the kinetic energy of the electron. Hence, $mv_f^2=mv_i^2-2\Delta E$, where m is the electron mass. The direction of $\mathbf{v}_f$ is given by the electron-scattering angles (θ,ϕ) as shown in Fig. 1. For any given set of the independent parameters $(v_N,u_i,\beta,\theta,\phi,\Delta E)$, the final velocity of the electron with respect to the hydrogen center of mass is determined. For nonrelativistic velocities we have $\mathbf{u}_f=\mathbf{v}_f-\mathbf{v}_N$. The semiclassical condition for electron loss is that the electron acquires enough energy in the collision to exceed the ionization limit. Denoting the ionization energy of the ground-state hydrogen atom by E_I, the electron-loss condition is

$$mu_f^2 \geq mu_i^2+2E_I \ . \tag{1}$$

Expressing u_f in terms of the parameters $(v_N,u_i,\beta,\theta,\phi,\Delta E)$, the condition for electron loss is

$$A\sin\theta-B\cos\theta \geq C \ , \tag{2}$$

where

$$A\equiv\frac{u_i}{v_i}\sin\beta\cos\phi \ , \quad B\equiv\frac{1}{v_i}(v_N+u_i\cos\beta) \ ,$$

$$C\equiv\left[v_i^2-\frac{2\Delta E}{m}\right]^{-1/2}\left[\frac{E_I+\Delta E}{mv_N}-v_N-u_i\cos\beta\right]$$

and

$$v_i=(v_N^2+u_i^2+2u_iv_N\cos\beta)^{1/2} \ .$$

The total electron-loss cross section for a hydrogen atom incident on a target with velocity v_N is the sum of the differential cross sections leading to specific final atomic states j, integrated over ϕ and the allowed range of θ, and averaged over the initial distribution of electron velocities in the projectile,

$$Q(v_N)=\sum_j\int_0^\infty f(u_i)du_i \times\int_0^{\pi}\tfrac{1}{2}\sin\beta\,d\beta \times\int_0^{2\pi}d\phi\int\sigma_j(v_i,\theta)\sin\theta\,d\theta \ , \tag{3}$$

where the last integral is carried out for all values of θ that satisfy Eq. (2). In Eq. (3), $f(u_i)$ denotes the normalized distribution of the magnitude of the electron velocity u_i about the center of mass of the hydrogen projectile, and $\sigma_j(v_i,\theta)$ is the differential electron-scattering cross section for the process j at an angle θ for an electron with velocity v_i incident on the target chosen. The differential cross sections σ_j describe elastic scattering ($\Delta E_j=0$) or the various inelastic processes ($\Delta E_j\neq 0$). The sum over j includes both the elastic and inelastic processes.

Calculations of $Q(v_N)$ using Eqs. (1)–(3) are cumbersome, because the different σ_j's depend on u_i and β through the velocity $v_i=(u_i^2+v_N^2+2u_iv_N\cos\beta)^{1/2}$, and because the limits of the θ integration depend on u_i, β, ϕ, and ΔE_j. In order to simplify the calculations, we make the high-energy approximation that $\sigma_j(v_i,\theta)=\sigma_j(v_N,\theta)$. Although the distribution function $f(u_i)$ is well known,[13] we further simplify the calculations by taking $\mathbf{u}_i$ equal in magnitude to the root-mean-square velocity of the $1s$ electron in the hydrogen atom, $u_{\rm rms}$; that is, we replace $f(u_i)$ by $\delta(u_i-u_{\rm rms})$. The direction of $\mathbf{u}_i$, which is described by the angle β, is still assumed to have the same probability for any value of β between 0 and π. The simplifications regarding σ_j and $f(u_i)$ reduce substantially the time required for numerical calculations of $Q(v_N)$.

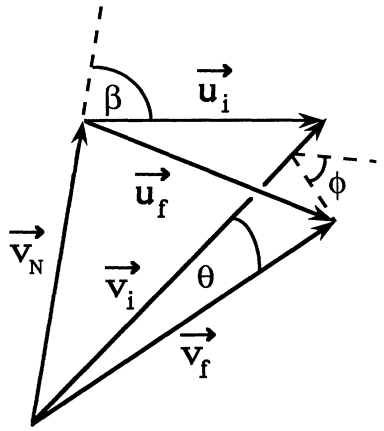

FIG. 1. Velocities and angles of the free-collision model in the laboratory frame in which the target is at rest. Velocities with respect to the center-of-mass system of the hydrogen projectile are denoted by $\mathbf{u}$, whereas velocities in the laboratory frame are denoted by $\mathbf{v}$. The subscripts i and f refer to initial and final velocity of the electron, respectively. The velocity of the projectile nucleus in the laboratory frame is $\mathbf{v}_N$. The electron-scattering angles in the laboratory frame are θ and ϕ. The angle θ is the angle between $\mathbf{v}_i$ and $\mathbf{v}_f$. The angle ϕ is the angle between the plane defined by $\mathbf{v}_N$ and $\mathbf{v}_i$ and the plane defined by $\mathbf{v}_i$ and $\mathbf{v}_f$. All values for the angle β between $\mathbf{u}_i$ and $\mathbf{v}_N$ are equally probable.

We restrict our calculations to those values of v_N where $v_N > u_{\rm rms}$; this means that our calculations are valid for incident H(1s) kinetic energies greater than 25 keV. Because we take $u_i = u_{\rm rms} < v_N$, the quantity B in Eq. (2) is always positive, and the integration limits can be stated in a simple way. Implementing the simplifications explained above, the electron-loss cross section is

$$Q(v_N) = \tfrac{1}{2}\sum_j \int_0^{\pi} \sin\beta\, d\beta \int_0^{2\pi} d\phi \int_{\theta_{c,j}}^{\pi} \sigma_j(v_N,\theta)\sin\theta\, d\theta \ , \tag{4}$$

where we have introduced the critical angle $\theta_{c,j}$ as the lower integration limit. The critical angle is given by

$$\theta_{c,j} = \begin{cases} 0 & \text{for } y > 1 \\ \cos^{-1} y & \text{for } -1 \le y \le 1 \\ \pi & \text{for } y < -1 \ , \end{cases} \tag{5}$$

where

$$y = [\,A(A^2+B^2-C^2)^{1/2} - BC\,](A^2+B^2)^{-1} \ .$$

Here, A, B, and C must be evaluated for $u_i = u_{\rm rms}$ and $\Delta E = \Delta E_j$. Physically, the critical angle $\theta_{c,j}$ is such that electron detachment occurs if the electron-scattering angle θ is greater than $\theta_{c,j}$. It should be noted that $\theta_{c,j}$ is a function of β, ϕ, and ΔE_j.

For $u_{\rm rms} \ll v_N$, the calculation can be further simplified if Eq. (2) is expanded in terms of $u_{\rm rms}/v_N$ and θ, keeping terms up to order $u_{\rm rms}^2/v_N^2$ and θ^2. For small angles θ, this yields an expression quadratic in θ^2, and the critical angle is then given by

$$\theta_c = \frac{u_{\rm rms}}{v_N}[(1+\sin^2\beta\cos^2\phi)^{1/2} - \sin\beta\cos\phi]$$
$$= \frac{u_{\rm rms}}{v_N}[(1+x^2)^{1/2} - x] \ , \tag{6}$$

where $x = \sin\beta\cos\phi$. This result is consistent with the assumption of θ being a small angle and $u_{\rm rms} \ll v_N$. In this approximation θ_c is independent of ΔE_j, and is only a function of x. Making a variable transformation from (β,ϕ) to $(\cos\beta, x)$, the $\cos\beta$ dependence can be integrated out, and the final result for the electron-loss cross section in the high-energy approximation assumes the simple form

$$Q(v_N) = \pi \int_{-1}^{1} dx \int_{\theta_c(x)}^{\pi} \sum_j \sigma_j(v_N,\theta)\sin\theta\, d\theta \ , \tag{7}$$

where θ_c is the same for all the different electron-scattering processes j.

At sufficiently high energies relativistic effects must also be included. In this situation the laboratory frame, in which the target is at rest, is related to the projectile center-of-mass frame by a Lorentz transformation with $\gamma = [1-(v_N/c)^2]^{-1/2}$. Using the Lorentz transformation, we can relate $\mathbf{u}_i$ to $\mathbf{v}_i$ and $\mathbf{u}_f$ to $\mathbf{v}_f$. We include the relativistic corrections to $\theta_c(x)$ so that our calculations are correct even at energies up to 1.4 GeV.

III. CALCULATED ELECTRON-LOSS CROSS SECTIONS FOR AN INCIDENT H(1s) PROJECTILE

We have calculated the electron-loss cross sections for H(1s) incident on atomic targets of He, Ne, Ar, Kr, Xe, H, N, and O as follows. At low energies, we should properly use Eqs. (4) and (5) to calculate $Q(v_N)$, while at high energies we may use Eqs. (6) and (7). In particular, the values of $\theta_{c,j}$ from Eq. (5) can differ from the value of $\theta_c(x)$ calculated from Eq. (6) by as much as 40% at an energy of 90 keV. However, with the extra angular averaging, the cross sections obtained from Eq. (4) using the $\theta_{c,j}$'s differ from the cross sections obtained from Eq. (7) using the $\theta_c(x)$'s by less than 4%. At higher energies, the differences between $\theta_{c,j}$ and $\theta_c(x)$ and between the corresponding cross sections are still smaller. For this reason, we have actually used Eq. (7) to calculate $Q(v_N)$ for all energies from 90 keV to 1.4 GeV.

In order to use Eqs. (4) or (7), one must know the differential cross sections σ_j. The largest differential cross sections σ_j for the scattering of the nearly free electron by the target are those for elastic scattering ($\sigma_{\rm el}$), excitation of the target to the lowest excited level ($\sigma_{\rm exc}$), and ionization of the target to the lowest continuum level ($\sigma_{\rm ion}$). Hence, we truncate the sum in Eq. (7) to a sum over these three processes. To evaluate $Q(v_N)$ we then need $\sigma_{\rm el}$, $\sigma_{\rm exc}$, and $\sigma_{\rm ion}$ as functions of the incident electron energy and scattering angle. In the following two paragraphs, we give the origin of the differential electron-scattering cross sections used in our calculations.

A. Elastic differential cross sections

At low energies we utilize elastic differential electron-scattering cross sections calculated by McCarthy *et al.*[14] for all the inert-gas targets (20–3000-eV incident electron energies) and those by Blaha and Davis[15] for atomic oxygen and nitrogen targets (20–500-eV incident electron energies). At higher energies we utilize the Born-approximation calculations for the elastic-scattering cross sections with the elastic form factors calculated by Bonham and Schäfer[16] for all targets. Bonham and Schäfer have calculated form factors only at a few fixed energies. The form factors at energies between those given are obtained using an interpolation scheme similar to that given in Ref. 16. We use the elastic Born cross sections at electron energies high enough that the Born cross section is smaller than the cross sections calculated using a low-energy formalism. For example, we use the Born elastic cross section at incident electron energies above 3×10^3 eV for a He target and above 3×10^4 eV for a Xe target. For the atomic hydrogen target we use the Born elastic cross section at all energies. This gives an excellent fit to the experimental cross sections. It should be noted that the Born cross sections are neither scaled to fit experiment nor to fit our low-energy calculations, but are used directly as calculated from the form factors given by Bonham and Schäfer.

B. Inelastic differential cross sections

The inelastic excitation and ionization differential cross sections that we use in our calculations are obtained as follows. For the inert-gas targets and at low energies, we use the total inelastic excitation or ionization cross sections from de Heer, Jansen, and van der Kaay.[17] They obtained the total inelastic cross sections from a semiempirical combination of experimental data and theoretical calculations. Since their calculations are for total cross sections rather than differential cross sections, we assume that the angular dependence of the differential cross section at low energies is identical to the angular dependence of the Born inelastic cross section at low energies so that

$$\int_{\theta_c}^{\pi}\sigma_j d\Omega=\frac{Q_j^{\text{deHeer}}\int_{\theta_c}^{\pi}\sigma^B d\Omega}{\int_0^{\pi}\sigma^B d\Omega} . \tag{8}$$

Here, Q_j^{deHeer} is the total cross section for process j, where j stands for excitation (j=exc) or ionization (j=ion), provided by de Heer, Jansen, and van der Kaay,[17] and σ^B is the inelastic differential cross section in the Born approximation with the form factors given by Bonham and Schäfer.[16] We use the semiempirical cross sections of de Heer, Jansen, and van der Kaay at energies low enough that $Q_{\text{exc}}^{\text{deHeer}}+Q_{\text{ion}}^{\text{deHeer}}<\int_0^{\pi}\sigma^B d\Omega$, and we use the Born inelastic cross sections at higher energies where the inequality is reversed. This procedure results in our using the Born inelastic cross sections at electron energies above 300 eV for a He target and above 2000 eV for a Xe target. For atomic O and N targets there are no differential or total inelastic cross sections for the low-energy region of our calculations. Our calculations for low energies are based only on the differential elastic-scattering cross sections, and therefore represent only a lower limit for the total cross section, $Q(v_N)$. For atomic hydrogen targets, the Born approximation with the inelastic form factors given by Bonham and Schäfer[16] is used at all energies, as was done for the elastic case. At high energies, for all targets, we use the Born inelastic differential cross sections with the form factors again given by Bonham and Schäfer.[16]

Our numerically calculated cross sections together with the corresponding experimental results are shown as functions of the energy of the incident hydrogen projectile in Fig. 2. As can be seen, the agreement of our calculations with experimentally measured cross sections is remarkably good. For further experimental results we refer to the review articles given in Ref. 24.

IV. SINGLE- AND DOUBLE-ELECTRON-LOSS CROSS SECTIONS FOR H^-

In this section, we present calculations of both the single- and double-electron-loss cross sections for H^- ions incident on the same target gases as used in the H(1s) electron-loss calculations. The electron loss for H^- is semiclassically described in two steps. Assuming that there is no correlation between the two electrons, the first step is that each electron will independently be subject to hard scattering, identical to the electron scattering in the case of an incident H atom. This hard-scattering process can lead to no-, single-, or double-electron loss. If there

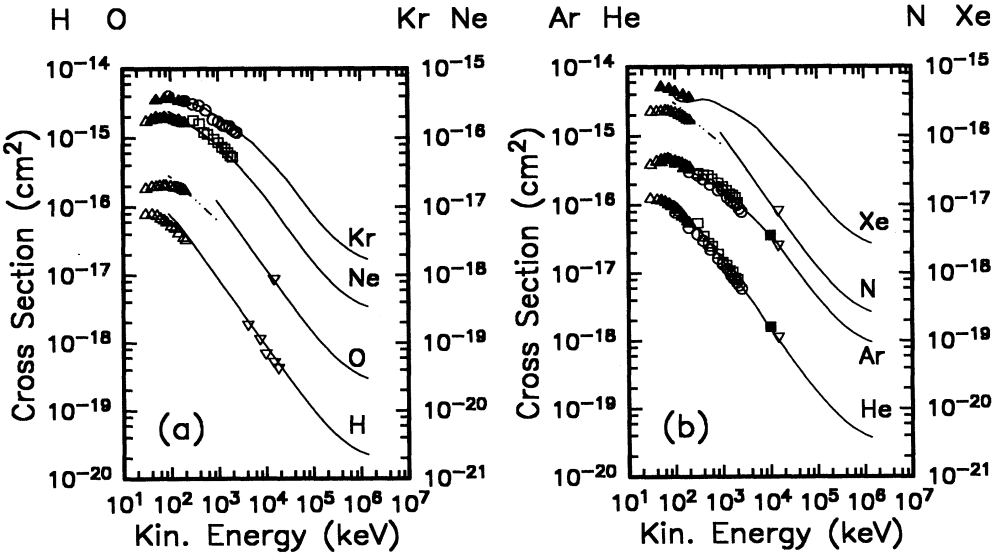

FIG. 2. Electron-loss cross sections of H(1s) incident on He, Ne, Ar, Kr, Xe, and atomic H, N, and O targets as a function of the kinetic energy of the incident H(1s) projectile. The solid lines are the calculated electron-loss cross sections including elastic- and inelastic-scattering processes, and the dot-dashed lines are the calculated electron-loss cross sections based only on elastic electron scattering. The symnbols represent experimental measurements and are taken from Ref. 18 (open triangle), Ref. 19 (open square), Ref. 20 (open inverted triangle), Ref. 21 (open circle), Ref. 22 (solid triangle), and Ref. 23 (solid square). Our calculations are only carried out for energies above 90 keV. However, we show experimental data at energies below 90 keV to indicate the trend of the experimental data.

is no electron loss due to the hard scattering, the electrons are assumed to remain in their initial wave function, and the electron-loss cross section vanishes. If one electron is lost due to hard scattering, the remaining electron will be left in a state that is not an eigenstate of H^0. Hence the remaining electron may undergo a transition into either a continuum state ("electron shake-off") or to a bound state. In the first case, the whole two-step process contributes to the total double-electron-loss cross section. In the second case, it contributes to single-electron loss. The final possibility is that both electrons are lost in the hard-scattering process, a process that contributes directly to the double-electron-loss cross section.

We first calculate the hard-scattering cross sections utilizing the classical-impulse approximation in the context of the eikonal formulation of scattering theory. We assume that the two electrons scatter independently, so that the free-collision model previously applied to the electron of H(1s) can now be applied to each of the two electrons in H^- separately. We take one electron to be bound by 0.75 eV and the other by 13.6 eV. The electron-loss cross section Q_1 for hard scattering of the tightly bound electron is given by the results of the preceding section. The electron-loss cross section Q_2 for hard scattering of the loosely bound electron is obtained from similar calculations carried out for an ionization energy of 0.75 eV and using the corresponding $u_{\rm rms}$ for the loosely bound electron. This yields values of Q_2 which are 1.4 to 3.0 times larger than the corresponding values of Q_1. The electron-loss cross sections Q_1 and Q_2 are hard-interaction cross sections, which means that Q_i describes the electron loss of electron i due to direct scattering on the target atom, independent of whether the other electron is detached during the hard scattering or not. Following the ideas of Bates and Walker[12] and Dewangan and Walters,[10] these two interaction cross sections for the hard process can be visualized as two disks of radius $l_i=(Q_i/\pi)^{1/2}$, where $i=1$ or 2. Again $i=1$ corresponds to the tightly bound electron and $i=2$ corresponds to the loosely bound electron. As shown in Fig. 3, the two disks generally overlap. The overlap area A_0 depends on the distance d between the centers of the two disks. The distance d is given as the projection of the vector separation **R** of the two electrons on the plane perpendicular to the direction of incidence. The total cross-sectional area of the two electrons of the H^- ion from the perspective of the target is $Q_1+Q_2-A_0$. We interpret the overlap area

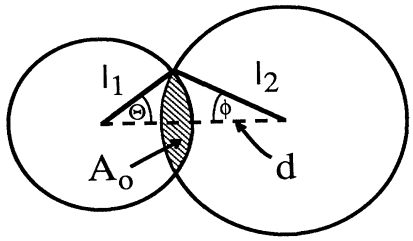

FIG. 3. Cross-sectional areas for electron loss presented to a target by an incoming H^- projectile.

A_0 as the double-electron-loss cross section associated with direct or hard scattering of both electrons. The remaining area, $Q_1+Q_2-2A_0$, is interpreted as the single-electron-loss cross section for hard scattering. These results are formally derived in Appendix A using the eikonal formulation of scattering theory. In order to evaluate the single- and double-electron-loss cross sections, the overlap area A_0 must be averaged over all orientations and magnitudes of **R**. Hence we need a reasonable approximation for the electronic wave function $\psi(\mathbf{r}_1,\mathbf{r}_2)$ of H^- to extract the normalized distribution function $P(\mathbf{R})$ for the electron separation **R**. This is discussed in Appendix B.

The last step in calculating the double-electron loss is to choose the eikonal scattering function to determine the hard-scattering ionization probabilities. This is discussed in Appendix A. For a Gaussian distribution we obtain

$$\sigma_{\rm db}^{\rm hard}=\langle A_0\rangle = \tfrac{1}{2}\int_0^\infty dR\, P(R)\int_0^\pi d\theta(\sin\theta)\frac{Q_1Q_2}{Q_1+Q_2} \times\exp\left[-\frac{\pi R^2\sin^2\theta}{Q_1+Q_2}\right] . \quad (9)$$

For a step distribution we obtain

$$\sigma_{\rm db}^{\rm hard}=\langle A_0\rangle = \tfrac{1}{2}\int_0^\infty dR\, P(R)\int_0^\pi d\theta(\sin\theta)A_0(l_1,l_2,R\sin\theta) , \quad (10a)$$

where[25]

$$A_0(l_1,l_2,d)=\begin{cases}\pi l_1^2 & \text{for } d\le l_2-l_1\\ l_1^2(\theta-\sin\theta\cos\theta)+l_2^2(\phi-\sin\phi\cos\phi) & \text{for } (l_2-l_1)<d<(l_2+l_1)\\ 0 & \text{for } d\ge l_2+l_1\end{cases} \quad (10b)$$

with

$$\theta=\cos^{-1}\left[\frac{d^2+l_1^2-l_2^2}{2dl_1}\right] ,$$

$$\phi=\cos^{-1}\left[\frac{d^2+l_2^2-l_1^2}{2dl_2}\right] .$$

We compare the results for these two expressions for $\sigma_{\rm db}^{\rm hard}$ in the case of a H target and a Xe target in Fig. 4. Clearly, $\sigma_{\rm db}^{\rm hard}$ is insensitive to the choice of distribution.

The single-electron-loss cross section for electron i due to hard scattering is given as

$$\sigma_{{\rm sng},i}^{\rm hard}=Q_i-\langle A_0\rangle=Q_i-\sigma_{\rm db}^{\rm hard} . \quad (11)$$

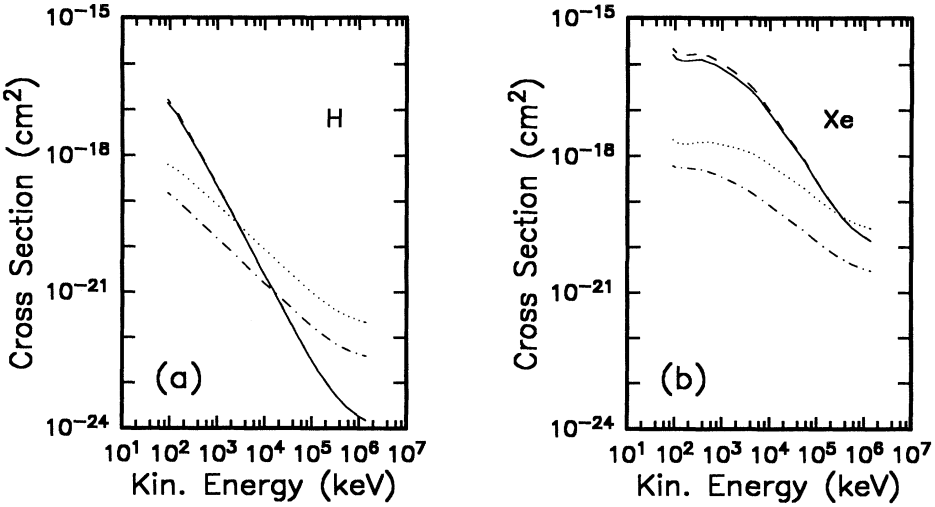

FIG. 4. Contributions to Q_{db} for (a) a H target, and (b) a Xe target. The solid line represents σ_{db}^{hard} as calculated using a Gaussian eikonal function [see Eq. (9)], and the dashed line represents σ_{db}^{hard} based on a step function for the eikonal distribution [see Eq. (10)]. The dotted line shows the contribution to Q_{db} from shake-off of the remaining loosely bound electron $(Q_1-\sigma_{db}^{hard})P_2$, calculated with $P_2=9.63\times10^{-3}$ and the hard cross section for the Gaussian eikonal distribution. The dashed-dotted line is the corresponding contribution from shake-off of the tightly bound electron $(Q_2-\sigma_{db}^{hard})P_1$, with $P_1=6.6\times10^{-4}$. Note that the shake-off cross section becomes increasingly important at high energies, and can be larger than σ_{db}^{hard} for a light (H) target. It is relatively less important for a heavy (Xe) target.

However, an electron can also be lost through the shake-off process noted above even if it does not interact directly with the target atom. As discussed in Appendix B, our choice for the initial H^- wave function is a symmetrized wave function of the form $\psi(\mathbf{r}_1,\mathbf{r}_2)=N[\phi(Z_1,\mathbf{r}_1)\phi(Z_2,\mathbf{r}_2)+\phi(Z_1,\mathbf{r}_2)\phi(Z_2,\mathbf{r}_1)]$. We have assumed that scattering of one electron on the target atom does not influence the other electron. Hence, if one electron is removed, the remaining electron will be left in a state $\phi(Z_i,\mathbf{r})$ which, in general, is not an eigenstate of H^0. The probability P_i that the remaining electron will make a transition into a continuum state, that is, will be "shaken off" in the overall process, is given by

$$P_i=\int d^3p\frac{1}{(2\pi)^3}\left|\int R(\mathbf{p},\mathbf{r})\phi(Z_i,\mathbf{r})d^3r\right|^2,$$

where $R(\mathbf{p},\mathbf{r})$ is a properly normalized continuum-state wave function for an electron of momentum $\mathbf{p}$ in the Coulomb field of hydrogen nucleus. Choosing

$$\phi(Z_i,\mathbf{r})=\left[\frac{Z_i^3}{\pi}\right]^{1/2}e^{-Z_ir},$$

we obtain

$$P_i=\frac{32}{Z_i}\left[1-\frac{1}{Z_i}\right]^2\times\int_0^\infty dt\frac{t}{(1+t^2)^4}\left[\sinh\frac{\pi}{Z_it}\right]^{-1}\times\exp\left[-\frac{4}{Z_it}\left[\frac{\pi}{4}-\tan^{-1}\frac{1}{t}\right]\right]. \quad (12)$$

In Fig. 5 we show P_i as a function of Z_i. As explained in Appendix B, we choose $Z_1=1.0445$ and $Z_2=0.3259$ as the best values for the calculation of $P(R)$. This choice gives $P_1=6.55\times10^{-4}$ and $P_2=9.63\times10^{-3}$, respectively. The shake-off cross sections are then

$$\sigma_1^{\text{shake-off}}=P_1\sigma_{\text{sng},2}^{\text{hard}}=P_1(Q_2-\langle A_0\rangle),$$
$$\sigma_2^{\text{shake-off}}=P_2\sigma_{\text{sng},1}^{\text{hard}}=P_2(Q_1-\langle A_0\rangle). \quad (13)$$

The probability that electron i is *not* shaken off is $1-P_i$, so the total single-electron-loss cross section is

$$Q_{\text{sng}}=(1-P_2)\sigma_{\text{sng},1}^{\text{hard}}+(1-P_1)\sigma_{\text{sng},2}^{\text{hard}}=(1-P_2)Q_1+(1-P_1)Q_2-(2-P_1-P_2)\langle A_0\rangle. \quad (14)$$

Finally, the double ionization cross section with shake-off included is

$$Q_{\text{db}}=\sigma_{\text{db}}^{\text{hard}}+P_2\sigma_{\text{sng},1}^{\text{hard}}+P_1\sigma_{\text{sng},2}^{\text{hard}}=(1-P_1-P_2)\langle A_0\rangle+P_2Q_1+P_1Q_2. \quad (15)$$

The quantities that we actually calculate are $Q_1,Q_2,\langle A_0\rangle$ and P_1,P_2.

In Fig. 4 we show the calculated results for the individual shake-off cross sections $(1-P_1)\sigma_{\text{sng},2}^{\text{hard}}$ and $(1-P_2)\sigma_{\text{sng},1}^{\text{hard}}$ for the case of a H and Xe target. In each case, electron 2 is the weakly bound electron, and has the larger shake-off cross section. The cross sections $\sigma_{\text{sng},1}^{\text{hard}}$ and $\sigma_{\text{sng},2}^{\text{hard}}$ used are based on a Gaussian distribution function for calculating $\sigma_{\text{db}}^{\text{hard}}$ in an eikonal formalism [see Eq.

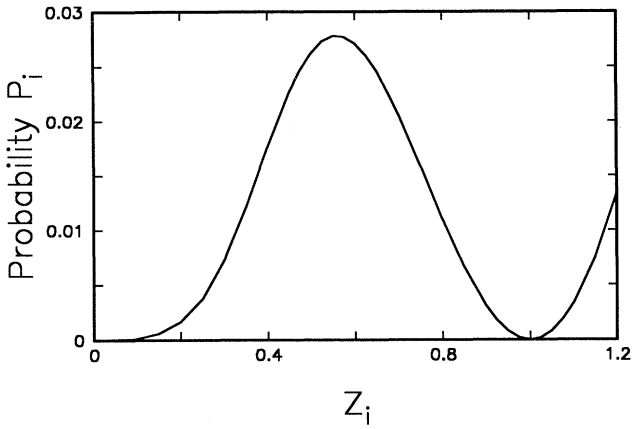

FIG. 5. The transition probability P_i as a function of the parameter Z_i of the electron wave function. The curve was calculated using Eq. (12).

(9) and Appendix A].

In Figs. 6 and 7 we compare the total cross sections $Q_{\rm sng}$ and $Q_{\rm db}$ calculated using $\sigma_{\rm db}^{\rm hard}$ of Eq. (9) for the different atomic gas targets H, He, Ne, Ar, Kr, Xe, N, and O to the relevant experimental cross sections. As can be seen, the agreement of the theoretical results with the experimental cross sections for both single- and double-electron loss is astonishingly good. At very high energies, our results for the double-electron-loss cross sections are somewhat too low, though it should be pointed out that the experimental results are subject to uncertainties of about 25%.

One might expect that our model should be more reliable at higher energies since the approximations used in calculating the cross sections Q_1 and Q_2 should become more accurate for v_N much larger than $u_{\rm rms}$. A few sample calculations, which included the u_i average, rather than taking $u_i = u_{\rm rms}$, differed from the simplified calculations by less than 4% for the high-energy case. We therefore conclude that more complete calculations, which utilize Eq. (3) in context with the eikonal model described above, are unlikely to eliminate the apparent discrepancy between the theoretical and experimental results for the high-energy double-electron-loss cross sections. It is therefore possible that the present model has to be extended. For example, correlation effects between the two electrons, or electron-electron scattering inside the perturbed H^- system, could enhance the double-electron-loss cross section without significantly changing the single-electron-loss cross section. It would certainly be of interest to have more data, including data at even higher energies than the present limits, so that the general energy dependence of the cross sections can be checked, and the theory refined.

V. H(1s) ELECTRON-LOSS CROSS SECTIONS FOR MOLECULAR TARGETS

We have also calculated the single-electron-loss cross section for H(1s) atoms incident on molecular gas targets

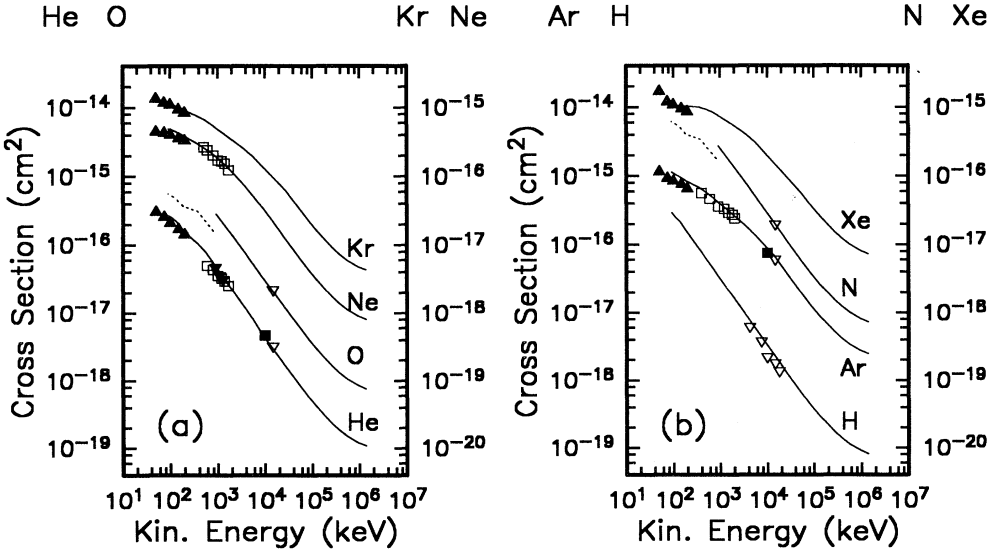

FIG. 6. Single-electron-loss cross sections of H^- incident on He, Ne, Ar, Kr, Xe, and atomic H, N, and O targets as a function of the energy of the incident H^- projectile. The solid lines are the single-electron-loss cross sections calculated from single-electron-scattering cross sections, which include both elastic- and inelastic-scattering processes. Electron shake-off corrections are included. The dotted lines are the calculated single-electron-loss cross sections only based on elastic electron scattering. The symbols represent experimental measurements and are taken from Ref. 19 (open square), Ref. 20 (open inverted triangle), Ref. 22 (solid triangle), Ref. 23 (solid square), and Ref. 26 (solid inverted triangle).

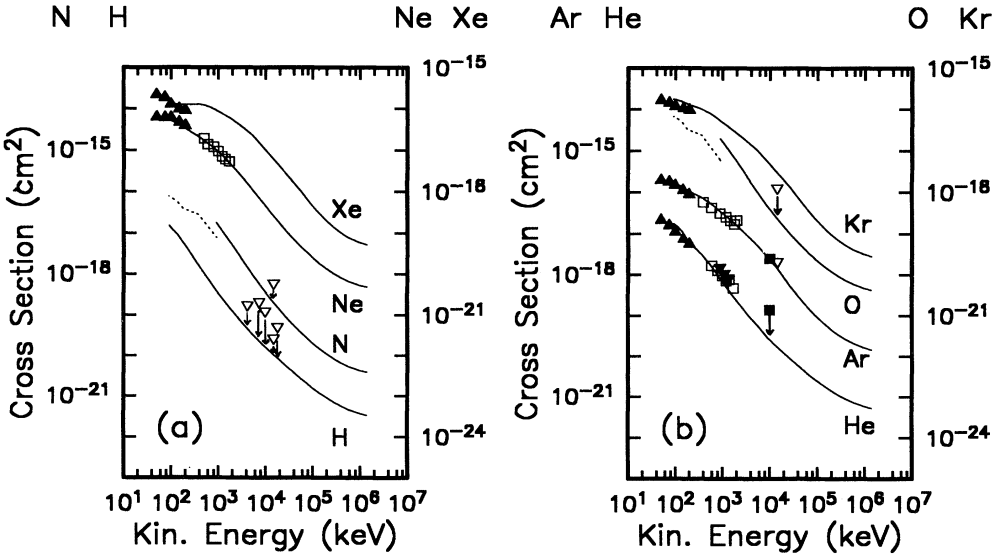

FIG. 7. Double-electron-loss cross sections of H^- incident on He, Ne, Ar, Kr, Xe, and atomic H, N, and O targets as a function of the energy of the incident H^- projectile. The solid lines are the double-electron-loss cross sections calculated from single-electron-scattering cross sections, which include both elastic- and inelastic-scattering processes. Electron shake-off contributions are included. The dotted lines are the calculated double-electron-loss cross sections based on elastic single-electron scattering alone. The symbols represent experimental measurements and are taken from Ref. 19 (open square), Ref. 20 (open inverted triangle), Ref. 22 (solid triangle), Ref. 23 (solid square), and Ref. 26 (solid inverted triangle). Where necessary we use arrows to indicate to which curve the experimental data correspond.

H_2, N_2, or O_2 using the results from the calculations for atomic H, N, or O targets. We take Q to be the cross section for one of the atoms in the diatomic molecule as calculated in Sec. III. The electron-loss cross section seen by the H(1s) atom incident on the diatomic homonuclear molecule is $Q_d = 2Q - A$, where A is the atomic overlap calculated in the Gaussian eikonal model using the analog of Eq. (9) with $Q_1 = Q_2 = Q$. The origin of the overlap can be visualized in this case as the result of one of the two atoms of the target molecule being behind the other from the perspective of the incident projectile. The overlap area A depends on the vector separation $\mathbf{R}$ of the two target atoms. To get the total electron-loss cross section, one must average Q_d over all possible spatial orientations of $\mathbf{R}$, as well as over the different allowed magnitudes of $\mathbf{R}$ due to vibration. We average the overlap area A only over the angular distribution. Each orientation of $\mathbf{R}$ is assumed to be equally probable. Because the amplitudes of vibrations about the mean interatomic separations are small, we approximate $P(R)$ in Eq. (9) by $\delta(R - R_{\rm av})$, where $R_{\rm av}$ is the average value for the internuclear separation: $R_{\rm av} = 0.7461$, 1.0975, and 1.208 Å for H_2, N_2, and O_2, respectively.[27]

The quantity of interest is the ratio of the electron-loss cross section for H(1s) incident on a diatomic target divided by the electron-loss cross section for H(1s) incident on a monatomic target. The ratios are shown for H_2, N_2, and O_2 as functions of the kinetic energy of the incident H(1s) atom in Fig. 8. At high energies, $(Q/\pi)^{1/2}$ is small compared to the internuclear distance, the overlap area is small, and the ratio is close to 2, as would be expected. At low energies, $(Q/\pi)^{1/2}$ is large compared to the internuclear distance, the overlap area is large, and the ratio is significantly below 2.

The comparisons of our calculations with previous experimental data are shown in Fig. 9. The very good agreement of the calculated and measured cross sections implies that one can extract reliable atomic cross sections from molecular cross sections by using the theoretical molecular-to-atomic cross section ratios discussed above. Often experiments are more easily carried out using a molecular gas target rather than an atomic gas target.

VI. CONCLUSIONS AND DISCUSSION

In this section, we briefly discuss our calculations and compare them with previous theoretical calculations. Except for some of the high-energy results for double-electron-loss cross sections of H^-, the agreement of our calculated electron-loss cross sections with the experimental data is remarkably good for H(1s) and H^- projectiles. Based on this agreement, we expect that the calculated cross sections are likely to be correct at energies where there are no experimental data available.

The experimental cross sections for single electron loss from H^- in Ar, Kr, or Xe show the following interesting

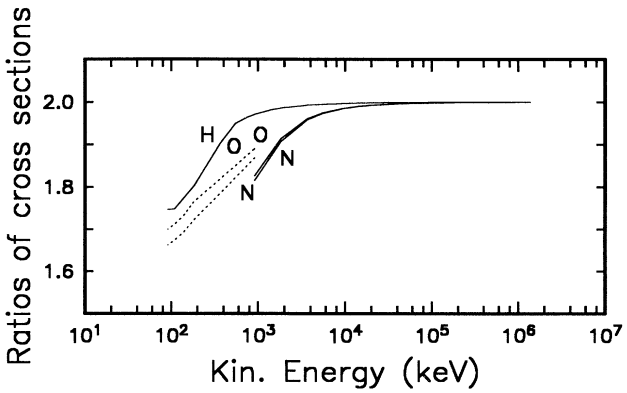

FIG. 8. Ratio of the electron-loss cross section for H(1*s*) incident on a diatomic target to the electron-loss cross section for H(1*s*) incident on a monatomic target for different energies of the incident H(1*s*) projectile. Results are shown for the ratio of the molecular H_2, N_2, and O_2 targets to the corresponding monatomic targets. See Fig. 9 for the cross sections used to calculate the ratio. The solid lines correspond to calculations for H, O, and N in which the single-electron cross sections include both inelastic and elastic scattering. The dotted lines correspond to calculations for O and N that are based only on elastic electron scattering.

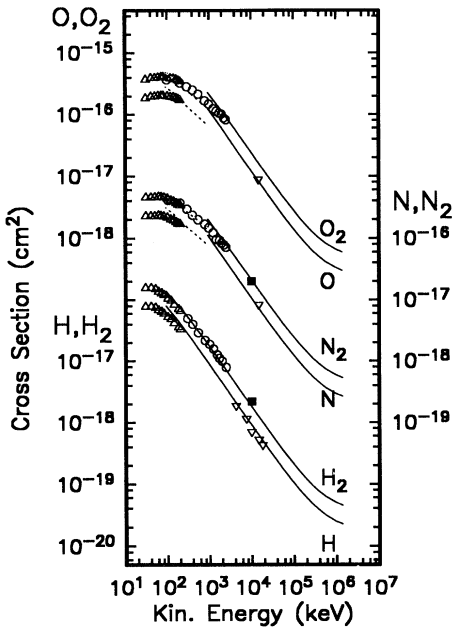

FIG. 9. Electron-loss cross sections of H(1*s*) incident on H, H_2, N, N_2, O, O_2 as a function of the energy of the incident H(1*s*) projectile. The solid lines are the calculated electron-loss cross sections calculated using single-electron scattering cross sections, which include both elastic- and inelastic-scattering processes. The dashed lines are the calculated electron-loss cross sections based on elastic single-electron-scattering cross sections. The symbols represent experimental measurements. For monatomic targets, they are taken from Ref. 18 (open triangle) and Ref. 20 (open inverted triangle), and for diatomic targets the results are from Ref. 18 (open triangle), Ref. 21 (open circle), and Ref. 23 (solid square). Reference 18 gives the electron-loss cross sections per target atom, but those results were obtained for H(1*s*) incident on diatomic targets multiplying the molecular results by a factor 0.5. Both results are shown.

feature.[22] At kinetic energies of about 100 keV the single-electron-loss cross section of H^- for a Kr target is larger than the corresponding cross section for a Xe target, and both are larger than the cross section for an Ar target. The increasing order is Ar-Xe-Kr. This seems surprising since the target sizes increase in the order Ar-Kr-Xe, and an ordering of the cross sections in the same way might be expected. For energies larger than approximately 200 keV, the measured single-electron-loss cross sections of H^- show the expected order. This interesting feature also shows up in our calculations.

In the case of electron loss from H(1*s*) incident on Ar, Kr, or Xe targets, the experimental results show a similar behavior.[22] At 100 keV the cross sections increase in the order Kr-Ar-Xe. For energies larger than approximately 200 keV the order Ar-Kr-Xe is observed as one might expect. Our calculations give a different result. At 100 keV they predict an increase of the electron-loss cross sections in the order Xe-Kr-Ar, and the order Ar-Kr-Xe is obtained for energies larger than 300 keV.

It is remarkable that our theoretical calculations give results that violate the order of cross-section magnitudes that one might expect from the size of the target atoms. The reason is that the theoretical electron differential cross sections by McCarthy *et al.*[14] have deep minima at certain angles. Because only the differential cross sections for angles larger than certain values of θ_c contribute to the total electron-loss cross section, the location of the minima is very important. Hence it is possible that, though the total electron-scattering cross section for angles from 0 to π for a Kr target is larger than for an Ar target, the electron-loss cross section of H(1*s*) for these targets is not. Because the calculations involve an average over $\theta_c(x)$, the final order of the results is not always easily predictable. In the case of H^- ions, the situation is even more difficult because there are two different θ_c's corresponding to a tightly and a loosely bound electron. Additionally, a three-dimensional averaging is needed in the H^- case to explain the measured cross sections.

To calculate H(1*s*) electron-loss cross sections, Dewangan and Walters[10] have utilized the free-collision model but with (in our notation) $u_i=0$. This is a satisfactory approximation at high energies. At low energies the agreement of some—but not all—cross sections with experiment is improved if one takes $u_i=u_{\rm rms}$ and takes all values of β as equally probable. Bates, Dose, and Young[11] have used the exact velocity distribution $f(u_i)$ rather than taking $u_i=u_{\rm rms}$. This is unquestionably the better approach, but since the free-collision model with $u_i=u_{\rm rms}$, and all values of β as equally probable gives remarkably good agreement with experiment, we believe

that for most cross sections our simplifying approximation is satisfactory. A considerable increase in computation time is required for the use of the exact distribution $f(u_i)$.

For the single- and double-electron-loss cross sections of H^- incident on atomic targets, our analysis is somewhat different from that of Bates and Walker[12] or Dewangan and Walters.[10] They both take the two electrons as having a mean projection $d=\langle R/2\rangle$ of the electron separation on the plane orthogonal to the incident velocity, where $\langle R\rangle$ is the mean electron separation in H^-. They then assign a cross section Q_i (where $i=1$ or 2) and hence a radius $l_i=(Q_i/\pi)^{1/2}$ to each electron. At low energies the radii are large enough that there is an overlap. At high energies, however, the radii are small and there is no overlap. On the other hand, we take a true three-dimensional average over the direction and magnitude of the separation $\mathbf{R}$ of the two electrons. In this case there is always a contribution to the overlap area when one electron is behind the other, even in the case of small radii, l_i. We have also shown formally that the overlap area is associated with the double electron loss. At high energies double electron loss due to shake-off contributes significantly to the total double electron loss. At low energies we obtain double-electron-loss cross sections that agree very well with experimental data. Even at high energies we obtain double-electron-loss cross sections that agree reasonably well with experimental data. We conclude that taking a three-dimensional average is important and offers a reasonable approximation for calculations of the double-electron-loss cross section in the classical-impulse approximation. A final judgment on the correctness of the double-electron-loss cross section results must be delayed until further high-energy experiments have been made.

Finally, if printed tables of the calculated cross sections are desired, they can be obtained by writing to the authors of this paper.

ACKNOWLEDGMENTS

We acknowledge support of this research by a grant from IBM Corporation to the University of Wisconsin, by National Science Foundation Grant No. PHY-8821097, and U.S. Department of Energy Contract No. AC02-76ER-00881. One of the authors (K.R.) would like to acknowledge additional support from the Studienstiftung des Deutschen Volkes, Federal Republic of Germany. We also acknowledge helpful conversations with John Magerlein, Tom Holley, and Dean Cirielli. One of the authors (K.R.) would also like to thank IBM for the hospitality granted during a research visit at the Thomas J. Watson Research Center. Another (L.D.) would like to thank the Aspen Center for Physics for its hospitality while parts of this work were done.

APPENDIX A

In this appendix we provide a brief discussion of the hard cross sections for single- and double-electron-loss cross sections from H^-. These cross sections, due to hard scattering, are $\sigma_{\rm db}^{\rm hard}=\langle A_0\rangle$ and $\sigma_{\rm sng}^{\rm hard}=Q_1+Q_2-2\langle A_0\rangle$. These expressions can be derived exactly and very simply, including the average over $\mathbf{R}$, in the impact-parameter approximation we have used. Assuming that the scattering of one electron is independent of the scattering of the other electron, the inelastic ionization cross section in the Glauber eikonal approximation is

$$\sigma_{\rm inel}=\int d^3r_1\int d^3r_2\int d^2b\,|\psi(\mathbf{r}_1,\mathbf{r}_2)|^2\times(1-e^{-2\,{\rm Re}\chi_1-2\,{\rm Re}\chi_2})\ , \tag{A1}$$

where ψ is the initial electron wave function, $\mathbf{r}_i=(\mathbf{b}_i,z_i)$ is the position of electron i with respect to the origin of the H^- center of mass, and $\mathbf{b}$ is the two-dimensional impact parameter of the H^- ion relative to the target atom. The eikonal functions χ_i describe the (independent) scattering of the electrons on the target atom. In particular, χ_i depends only on the impact parameter $\mathbf{b}_i'=\mathbf{b}-\mathbf{b}_i$ of electron i relative to the target, $\chi_i=\chi_i(\mathbf{b}_i')=\chi_i(\mathbf{b}-\mathbf{b}_i)$, where $\mathbf{b}$ is the ion-target impact parameter and $\mathbf{b}_i$ is the transverse coordinate of the electron in the incident ion. The function $e^{-2\,{\rm Re}\chi_i(\mathbf{b}-\mathbf{b}_i)}$ is equal semiclassically to the probability $\bar{p}_i(\mathbf{b}_i')$ that electron i does *not* undergo a hard, ionizing collision with the target atom for the given $\mathbf{b}$ and $\mathbf{b}_i$, independent of whether the other electron interacts or not. Let $p_i(\mathbf{b}_i')=1-\bar{p}_i(\mathbf{b}_i')$ denote the probability that electron i *does* interact. Then

$$1-e^{-2\,{\rm Re}\chi_1-2\,{\rm Re}\chi_2}=1-\bar{p}_1(\mathbf{b}_1')\bar{p}_2(\mathbf{b}_2')=p_1+p_2-p_1p_2\ ,$$

where p_1p_2 is the probability that *both* electrons interact directly with the target atom. Using this expression in Eq. (A1), we find that

$$\sigma_{\rm inel}=Q_1+Q_2-\sigma_{\rm db}^{\rm hard}\ , \tag{A2}$$

where

$$Q_i=\int d^3r_1\int d^3r_2\,|\psi(\mathbf{r}_1,\mathbf{r}_2)|^2\int d^2b\,p_i(\mathbf{b}-\mathbf{b}_i)=\int d^2b'\,p_i(\mathbf{b}')\tag{A3}$$

is just the interaction cross section for electron i, and

$$\sigma_{\rm db}^{\rm hard}=\langle A_0\rangle=\int d^3r_1\int d^3r_2\int d^2b\,|\psi(\mathbf{r}_1,\mathbf{r}_2)|^2\times p_1(\mathbf{b}-\mathbf{b}_1)p_2(\mathbf{b}-\mathbf{b}_2)\ . \tag{A4}$$

Alternatively, we can reexpress the eikonal probability function in Eq. (A1) as

$$1-e^{-2\,{\rm Re}\chi_1-2\,{\rm Re}\chi_2}=p_1\bar{p}_2+\bar{p}_1p_2+p_1p_2$$

and write $\sigma_{\rm inel}$ in terms of the two single-interaction cross sections and the double-interaction cross section,

$$\sigma_{\rm inel}=\sigma_{{\rm sng},1}^{\rm hard}+\sigma_{{\rm sng},2}^{\rm hard}+\sigma_{\rm db}^{\rm hard}=\sigma_{\rm sng}^{\rm hard}+\sigma_{\rm db}^{\rm hard}\ , \tag{A5}$$

where

$$\sigma_{{\rm sng},i}^{\rm hard}=Q_i-\sigma_{\rm db}^{\rm hard}=Q_i-\langle A_0\rangle\ . \tag{A6}$$

By introducing new variables $\mathbf{b}'=\mathbf{b}-\mathbf{b}_1$ and $\mathbf{d}=\mathbf{b}_1-\mathbf{b}_2$, we may rewrite the general result for the double-electron-loss cross section due to hard scattering as

$$\sigma_{\rm db}^{\rm hard}=\frac{1}{4\pi}\int P(R)\,dR\,d\Omega_R\int d^2b' p_1(\mathbf{b}')p_2(\mathbf{b}'+\mathbf{d}) =\tfrac{1}{2}\int dR\,d(\cos\theta)P(R)A_0(R\sin\theta)\ , \tag{A7}$$

where

$$\frac{1}{4\pi}P(R)\,dR\,d\Omega_R\equiv\left[\int|\psi(\mathbf{r}_1,\mathbf{r}_1+\mathbf{R})|^2d^3r_1\right]R^2dR\,d\Omega_R\ . \tag{A8}$$

This construction shows that $\sigma_{\rm db}^{\rm hard}$ only depends on the functional form of the ionization probabilities p_i and the distribution function for the vector separation $\mathbf{R}$ between the two electrons. Again $\mathbf{d}$ is the projection of $\mathbf{R}$ on the plane perpendicular to the direction of the incoming H^- ion.

Two simple choices for the eikonal probabilities p_i are the following:

(a) Gaussian distribution:

$$p_i(\mathbf{b})=e^{-b^2/l_i^2}\ ;$$

(b) Step distribution:

$$p_i(\mathbf{b})=\begin{cases}1, & |\mathbf{b}|<l_i\\ 0, & |\mathbf{b}|>l_i\ .\end{cases}$$

For either choice, the parameters l_i are related to the cross sections Q_i calculated in the free-collision model by $l_i=(Q_i/\pi)^{1/2}$. The Gaussian distribution is more realistic; the step distribution leads directly to the overlapping disk picture discussed in Sec. IV. Using these distribution functions we obtain the results of Eqs. (9) and (10), respectively.

We can also get some insight into the double scattering cross section by using a simple Gaussian model for the radial separation of the electrons in H^-, $P(R)\propto R^2e^{-(R/a)^2}$. The integrals in Eqs. (A7) and (9) can then be evaluated analytically using the Gaussian model for the eikonal probabilities, with the result

$$\sigma_{\rm db}^{\rm hard}=\frac{Q_1Q_2}{Q_1+Q_2+\pi a^2}\ . \tag{A9}$$

The area πa^2 is characteristic of the H^- ion. The low-energy data for double-electron loss as shown in Fig. 7 are fit within 20% using $\pi a^2\simeq 7\times10^{-16}$ cm^2. [This value gives a slightly small result for the average separation of the electrons, but reproduces the location of the peak in $P(R)$ obtained with realistic wave functions (see Appendix B).] Because Q_1 and Q_2 are considerably smaller than πa^2, especially at higher energies, $\sigma_{\rm db}^{\rm hard}$ is small, and falls more rapidly than Q_1 or Q_2 as the energy is increased.

We can extract a useful estimate of $\sigma_{\rm db}^{\rm hard}$ from Eq. (A9) by noting that, because of the smallness of $\sigma_{\rm db}^{\rm hard}$,

$$Q_1+Q_2=\sigma_{\rm sng}^{\rm hard}+2\sigma_{\rm db}^{\rm hard}\approx\sigma_{\rm sng}^{\rm hard}\ ,$$

while $Q_1=Q(\mathrm{H})$. Thus,

$$\sigma_{\rm db}^{\rm hard}\approx\frac{Q(\mathrm{H})[\sigma_{\rm sng}^{\rm hard}(\mathrm{H}^-)-Q(\mathrm{H})]}{\sigma_{\rm sng}^{\rm hard}(\mathrm{H}^-)+\pi a^2}\ . \tag{A10}$$

If we neglect the electron shake-off correction in $Q_{\rm sng}(\mathrm{H}^-)$, Eq. (14), and add the larger shake-off correction P_2Q_1 in Eq. (15) (see Fig. 4), we obtain

$$\sigma_{\rm db}\approx P_2Q(H)+\frac{Q(\mathrm{H})[Q_{\rm sng}(\mathrm{H}^-)-Q(\mathrm{H})]}{Q_{\rm sng}(\mathrm{H}^-)+\pi a^2}\ . \tag{A11}$$

This relation works reasonably well for our calculated cross sections, and may be useful for estimating double-electron loss of H^- from the single-electron-loss cross sections of H and H^- for energies between 90 and 5000 keV. (It should be noted that the upper energy limit chosen is sensitive to the target element considered.)

APPENDIX B

To obtain an approximate distribution function $P(R)$ for the distance R between the two electrons of the H^- ion, we assume that the electronic wave function can be written as

$$\psi(\mathbf{r}_1,\mathbf{r}_2)=\sqrt{N}\,[\phi(Z_1,r_1)\phi(Z_2,r_2)+\phi(Z_1,r_2)\phi(Z_2,r_1)]\ ,$$

where

$$\phi(Z,r)=(Z^3/\pi)^{1/2}\exp(-Zr)$$

and

$$\sqrt{N}=\left[2+\frac{128Z_1^3Z_2^3}{(Z_1+Z_2)^6}\right]^{-1/2}\ .$$

Throughout this appendix, we assume lengths to be in atomic units. It has been shown that this wave function gives a bound state.[28] The probability of a separation R between the two electrons is

$$P(R,Z_1,Z_2)=\int|\psi(\mathbf{r}_1,\mathbf{r}_2)|^2d^3r_1R^2d\Omega_R =4NZ_1^3Z_2^3R\left[e^{-2Z_1R}\left[\frac{2Z_2R}{(Z_1^2-Z_2^2)^2}+\frac{4Z_1Z_2}{(Z_1^2-Z_2^2)^3}\right]+e^{-2Z_2R}\left[\frac{2Z_1R}{(Z_1^2-Z_2^2)^2}-\frac{4Z_1Z_2}{(Z_1^2-Z_2^2)^3}\right]\right] +\frac{N(Z_1+Z_2)^3}{24}e^{-(Z_1+Z_2)R}[3R^2+3(Z_1+Z_2)R^3+(Z_1+Z_2)^2R^4]\ . \tag{B1}$$

The mean separation between the two electrons is then obtained as

$$\langle R \rangle = 2N \left[\frac{3Z_1^4+9Z_1^3Z_2+11Z_1^2Z_2^2+9Z_1Z_2^3+3Z_2^4}{2Z_1Z_2(Z_1+Z_2)^3} + \frac{280Z_1^3Z_2^3}{(Z_1+Z_2)^7} \right] . \quad \text{(B2)}$$

The parameters Z_1 and Z_2 are chosen to give the exact value of $\langle R \rangle$, which is 4.4129 a.u.,[29] and to minimize the total electronic energy under this constraint. This is achieved with $Z_1=1.0445$ and $Z_2=0.3259$, which yields $E_{\text{tot}}=-13.94$ eV. This corresponds to an electron affinity of 0.34 eV. Because we only use this wave function to obtain a reasonable distribution $P(R)$, the deviation in the electron affinity from the correct value, 0.75 eV, is of no concern. We have carried out alternative calculations of $\sigma_{\text{db}}^{\text{hard}}$ for the distribution functions $P(R)$ obtained from different wave functions.[30] We find that $\sigma_{\text{db}}^{\text{hard}}$ is not sensitive to the (reasonable) wave functions chosen as long as $\langle R \rangle$ is adjusted to 4.4129 a.u.

[1] H. S. Staten, *Production and Neutralizaton of Negative Ions and Beams,* AIP Conf. Proc. No. 111, edited by K. Prelec (AIP, New York, 1984), p. 587.

[2] L. W. Anderson, Nucl. Instrum. Methods **167**, 363 (1979). This reference and the next six references discuss primarily the formation of polarized negative ion beams. Intense polarized protons can be produced by electron detachment from fast nuclear-polarized hydrogen atoms. Fast nuclear-polarized neutral hydrogen atoms can be produced by repeated attachment and detachment of polarized electrons. The cross sections calculated in this paper are important in these processes.

[3] L. W. Anderson, S. N. Kaplan, R. V. Pyle, L. Ruby, A. S. Schlachter, and J. W. Stearns, Phys. Rev. Lett. **52**, 609 (1984).

[4] L. W. Anderson, S. N. Kaplan, R. V. Pyle, L. Ruby, A. S. Schlachter, and J. W. Stearns, J. Phys. B **17**, L229 (1984).

[5] Y. Mori, in *High Energy Spin Physics,* AIP Conf. Proc. No. 187, edited by K. J. Heller (AIP, New York, 1989), p. 1200.

[6] C. D. P. Levy, W. M. Law, M. McDonald, and P. W. Schmor (Ref. 5), p. 1210.

[7] A. N. Zelenski (Ref. 5), p. 1208.

[8] R. L. York, O. B. van Dyck, D. R. S. Swenson, and D. Tupa, in Proceedings of the International Workshop on Polarized Ion Sources and Polarized Gas Jets, edited by Y. Mori [KEK Report No. 90-15, Tsukuba, Japan (1990)], p. 170.

[9] I. S. Dmitriev and V. S. Nikolaev, Zh. Eksp. Teor. Fiz. **44**, 660 (1963) [Sov. Phys.—JETP **17**, 447 (1963)].

[10] D. P. Dewangan and H. R. J. Walters, J. Phys. B **11**, 3983 (1978).

[11] D. R. Bates, V. Dose, and N. A. Young, J. Phys. B **2**, 930 (1969).

[12] D. R. Bates and J. C. G. Walker, Proc. Phys. Soc. London **90**, 333 (1967).

[13] R. A. Mapleton, Proc. Phys. Soc. London **87**, 219 (1966).

[14] I. E. McCarthy, C. J. Noble, B. A. Phillips, and A. D. Turnbull, Phys. Rev. A **15**, 2173 (1977).

[15] M. Blaha and J. David, Phys. Rev. A **12**, 2319 (1975).

[16] R. A. Bonham and L. Schäfer, in *International Tables for X-Ray Crystallography,* edited by J. A. Ibers and W. C. Hamilton (Kynoch, England, 1974), Vol. IV, p. 176.

[17] F. J. de Heer, R. H. J. Jansen, and W. van der Kaay, J. Phys. B **12**, 979 (1979).

[18] P. M. Stier and C. F. Barnett, Phys. Rev. **103**, 896 (1956).

[19] D. P. Almeida, N. V. de Castro Faria, F. L. Freire, Jr., E. C. Montenegro, and A. G. de Pinho, Phys. Rev. A **36**, 16 (1987).

[20] R. Smythe and J. W. Toevs, Phys. Rev. **139**, A16 (1965).

[21] L. H. Toburen, M. Y. Nakai, and R. A. Langley, Phys. Rev. **171**, 114 (1968).

[22] C. J. Anderson, R. J. Girnius, A. M. Howald, and L. W. Anderson, Phys. Rev. A **22**, 822 (1980).

[23] K. H. Berkner, S. N. Kaplan, and R. V. Pyle, Phys. Rev. **134**, A1461 (1964).

[24] H. Tawara and A. Russek, Rev. Mod. Phys. **45**, 178 (1973); S. K. Allison, *ibid.* **30**, 1137 (1958).

[25] I. N. Bronshtein and K. A. Semendyavev, *Handbook of Mathematics* (Van Nostrand Reinhold, New York, 1985), p. 176.

[26] G. I. Dimov and V. G. Dudnikov, Zh. Tekh. Fiz. **36**, 1239 (1966) [Sov. Phys.—Tech. Phys. **11**, 919 (1967)].

[27] *CRC Handbook of Chemistry and Physics,* edited by R. C. Weast and D. R. Lide (Chemical Rubber Company, Florida, 1989), p. F189.

[28] S. Chandrasekhar, Astrophys. J. **100**, 176 (1944); H. P. Shull and P. O. Löwdin, J. Chem. Phys. **25**, 1035 (1956).

[29] C. L. Pekeris, Phys. Rev. **126**, 1470 (1962).

[30] In addition to the H^- wave function with the form and parameters above, we carried out sample calculations using the parameters that minimize the total energy (Ref. 28) $Z_1=1.0392$ and $Z_2=0.2832$, and calculations with the radial distributions $P(R)$ calculated for the wave functions $\psi(\mathbf{r}_1,\mathbf{r}_2)=(Z^3/\pi)e^{-Zr_1}e^{-Zr_2}$, $Z=0.49$, $\langle R \rangle=4.41$ a.u., and $\psi(\mathbf{r}_1,\mathbf{r}_2)=N(e^{-Z_1r_1}e^{-Z_2r_2}+e^{-Z_1r_2}e^{-Z_2r_2})(1+cR)$, $Z_1=1.075$, $Z_2=0.478$, $c=0.312$, $\langle R \rangle=4.25$ a.u. The latter form of the H^- wave function was introduced by S. Chandrasekhar, Ref. 28. For the latter cases the results obtained for $\sigma_{\text{db}}^{\text{hard}}$ differed by less than 8% from the original results. For a further discussion of H^- wave functions we refer to *H.* Massey, *Negative Ions* (Cambridge University Press, Cambridge, 1976), p. 9.